Relaxation Paths and Dynamics of Photoexcited Polyene Chains: Evidence for Creation and Annihilation of Neutral Soliton Pairs

Marco Garavelli,*,† Barry R. Smith,‡ Michael J. Bearpark,‡ Fernando Bernardi,† Massimo Olivucci,*,§ and Michael A. Robb*,‡

Contribution from the Dipartimento di Chimica "G. Ciamician", Università di Bologna, Via Selmi 2, 40126 Bologna, Italy, Istituto di Chimica Organica, Università di Siena, Via Aldo Moro, 53100 Siena, Italy, and Department of Chemistry, King's College, London, Strand, London WC2R 2LS, U.K.

Received February 1, 2000. Revised Manuscript Received March 25, 2000

Abstract: In recent work, we have demonstrated that the excited-state paths for radiationless deactivation and trans → cis isomerization for a series of polyenes involve a point of conical intersection between the covalent excited and ground states. In this paper we show how motion through this point can "trigger" the production of a transient π-diradical species (on the ground state) featuring an inverted double bond/single bond pattern. The computations have been carried out using an ab initio CAS−SCF approach and a hybrid molecular mechanics−valence bond (MM−VB) force field on three polyenes of increasing chain length: hexa-1,3,5-triene, octa-1,3,5,7-tetraene, and dodeca-1,3,5,7,9,11-hexaene ($C_{12}H_{14}$). Our computations show that production of the π-diradical must be a general feature of photoexcited polyenes. The investigation of the geometrical and electronic structure of these species indicates that they correspond to a pair of neutral solitons carrying unpaired electrons. Semiclassical trajectory computations on the "minimal" polyacetylene model $C_{12}H_{14}$ are used to model the creation, evolution, and annihilation dynamics of these transient entities.

1. Introduction

In recent computational work[1] we have demonstrated that the excited-state minimum energy paths (MEPs)[2] for a series of conjugated linear polyenes (structure 1) are consistent with the

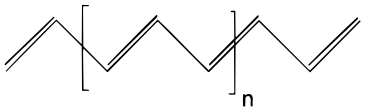

Structure 1

available experimental photochemical and photophysical data. These paths, on the potential energy surface of the $2A_g$ excited state (S_1), end at a point of real crossing with the $1A_g$ ground state (S_0) (throughout the paper we will use the C_{2h} symmetry labels of all-trans configurations). This crossing corresponds to an S_1/S_0 conical intersection.[3] The molecular structure at these conical intersections is characterized by an unusual out-of-plane distortion, a "kink" of a −CH−CH−CH− segment of the polyene chain. An example, the −C3−C4−C5− fragment of the conical intersection of octa-1,3,5,7-tetraene, is shown in Chart 1. This $-(CH)_3-$ kink is associated with an electronic configuration with three weekly coupled π-electrons (dashed lines in structure 2) which are localized on three adjacent −CH−

Chart 1

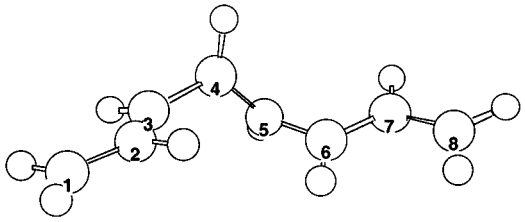

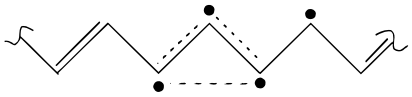

Structure 2

units and a fourth electron which is delocalized along a terminal segment of the conjugated chain.[1a] This type of conical intersection has been shown to provide the "funnel" for the fully efficient internal conversion from S_1 to the ground state of polyenes and subsequent transformations (e.g., cis−trans photoisomerization). Conical intersections also provide the radiationless decay channel for a large number of different organic molecules.[1,3]

In this paper we have investigated the internal conversion process, via the $-(CH)_3-$ kink type conical intersection, for

† Università di Bologna.
‡ King's College.
§ Università di Siena.

(1) (a) Celani, P.; Garavelli, M.; Ottani, S.; Bernardi, F.; Robb, M. A.; Olivucci, M. *J. Am. Chem. Soc.* **1995**, *117*, 11584. (b) Garavelli, M.; Celani, P.; Yamamoto, N.; Bernardi, F.; Robb, M. A. *J. Am. Chem. Soc.* **1996**, *118*, 11656. (c) Garavelli, M.; Celani, P.; Bernardi, F.; Robb, M. A.; Olivucci, M. *J. Am. Chem. Soc.* **1997**, *119*, 11487−11494. (d) Celani, P.; Bernardi, F.; Olivucci, M.; Robb, M. A. *J. Chem. Phys.* **1995**, *102*, 5733. (e) Bernardi, F.; Olivucci, M.; Robb, M. A. *Chem. Soc. Rev.* **1996**, *25*, 321 and references therein.

(2) Truhlar, D. G.; Steckler, R.; Gordon, M. S. *Chem. Rev.* **1987**, *87*, 217. Truhlar, D. G.; Gordon M. S. *Science* **1990**, *249*, 491.

(3) (a) Klessinger, M. *Angew. Chem., Int. Ed. Engl.* **1995**, *34*, 549. (b) Michl, J.; Bonacic-Koutecky, V. *Electronic Aspects of Organic Photochemistry*; Wiley: New York, 1990.

10.1021/ja000385l CCC: $19.00
Published on Web 05/26/2000

the S_1 excited state of *tZt*-C_6H_8 (*tZt*-hexa-1,3,5-triene), *all-trans*-C_8H_{10} (*all-trans*-octa-1,3,5,7-tetraene), and *all-trans*-$C_{12}H_{14}$ (*all-trans*-dodeca-1,3,5,7,9,11-hexaene) using unconstrained (i.e., all geometrical variables were included) MEP and trajectory computations. We show that deactivation through a S_1/S_0 conical intersection of this type either can lead to direct reactant back-formation (previously documented for *all-trans*-hexa-1,3,5-triene in ref 1c) or can trigger the production of a ground-state transient π-diradical species (i.e., an intermediate which does not correspond to a minimum), which then evolves to the original reactant via recoupling of the two radical centers. This paper is focused on the deactivation route involving the transient π-diradical species.

The computations have been carried out using both an ab initio CAS−SCF approach[4] (for the first two short polyene chains) and a hybrid molecular mechanics−valence bond (MM−VB) force field,[5] which enables us to compute the relaxation dynamics[6] for the longer polyene $C_{12}H_{14}$. We will show that the analysis of the MEP, and of the trajectories describing the deactivation process, provides information on the nature and stability of the transient species. In particular, we show that, after decay at an S_1/S_0 conical intersection, the system can populate decay paths characterized by highly twisted molecular arrangements showing single bond/double bond inversion and enhanced diradical character. In these structures, a significant section of the polyene chain, distinguished by an inverted coupling of the π-electrons, is sandwiched between two radical centers, as illustrated in structure 3. As we shall show

Structure 3

subsequently, these structures do not correspond to minima on the ground-state energy surface, but are transient π-diradical structures, which are located along a barrierless MEP which departs from the $-(CH)_3-$ kink conical intersection and ends at the original ground-state reactant well.

Hudson and Kohler[7b] have suggested that there is a strong analogy between the excited $2A_g$ state of polyenes and photo-induced "neutral soliton pairs"—a pair of quasi-localized chain deformations hosting radical centers—postulated to exist in long linear polyenes. A pair of neutral solitons formed on a finite *all-trans*-polyene is usually described by a planar (two-dimensional) structure where two radical centers are separated by a segment featuring an inverted double bond pattern. The

Chart 2

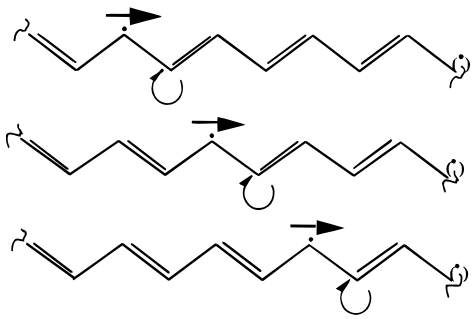

π-diradical transient species characterized in this paper provides the first fully unbiased model for the three-dimensional structure for a pair of neutral solitons. *This structure is very different from the planar structure postulated in the literature.*

A basic feature of solitons is that they are structural defects which undergo nondispersive shape-conserving motion.[8] For this reason solitons have been invoked in a wide variety of scientific applications mostly related to transport phenomena (such as conductivity and energy transfer) in polymers.[9] Neutral solitons are carriers of unpaired electrons, i.e., 1/2 spin carriers, which are believed to travel along a polyacetylene chain according to Chart 2.[9a−d]

Using $C_{12}H_{14}$, as a crude model of polyacetylene, we will document the emergence, propagation, and annihilation of the π-diradical transient species by means of semiclassical trajectory computations. We show that the position of the chain defects (i.e., the radical centers) and that of the associated inverted bonding segment change with time. The mechanism of radical transport and of the final annihilation of the two radical centers through electron spin recoupling will be documented in some detail, and we will show that the π-diradical (a pair of neutral solitons) can persist for several hundred femtoseconds. Analysis of our trajectory results suggests that the existence of this transient species is the result of a "dynamical locking" of the molecule in an orbit spanning a flat region of the S_0 energy surface. (For an interesting introduction to trapped or locked trajectories, which lie higher in energy than the barrier, in organic systems the reader is referred to the review of Carpenter.[6c])

(4) (a) Roos, B. O. *Adv. Chem. Phys.* **1987**, *69*, 399−446. (b) The MC−SCF program we used is implemented in Gaussian 94, Revision B.2: M. J. Frisch, G. W. Trucks, H. B. Schlegel, P. M. W. Gill, B. G. Johnson, M. A. Robb, J. R. Cheeseman, T. Keith, G. A. Petersson, J. A. Montgomery, K. Raghavachari, M. A. Al-Laham, V. G. Zakrzewski, J. V. Ortiz, J. B. Foresman, C. Y. Peng, P. Y. Ayala, W. Chen, M. W. Wong, J. L. Andres, E. S. Replogle, R. Gomperts, R. L. Martin, D. J. Fox, J. S. Binkley, D. J. Defrees, J. Baker, J. P. Stewart, M. Head-Gordon, C. Gonzalez, and J. A. Pople, Gaussian, Inc., Pittsburgh, PA, 1995.

(5) (a) Smith, B. R.; Bearpark, M. J.; Robb, M. A.; Bernardi, F.; Olivucci, M. *Chem. Phys. Lett.* **1995**, *242*, 27. (b) Bernardi, F.; Olivucci, M.; Robb, M. A. *J. Am. Chem. Soc.* **1992**, *114*, 1606.

(6) (a) Koppel, H.; Domcke, W.; Cederbaum, L. S. *Adv. Chem. Phys.* **1984**, *57*, 59. (b) Manthe, U.; Koppel, H. *J. Chem. Phys.* **1990**, *93*, 1658. (c) Carpenter, B. K. *Angew. Chem., Int. Ed.* **1998**, *37*, 3340.

(7) (a) Hudson, B. S.; Kohler, B. E.; Schulten, K. *Excited States* **1982**, *6*, 1. (b) Hudson, B. S.; Kohler, B. E. *Synth. Met.* **1984**, *9*, 241. (c) Kohler, B. E., Spangler, C.; Westerfield, C. *J. Chem. Phys.* **1988**, *89*, 5422. (d) Kohler, B. E. *Chem. Rev.* **1993**, *93*, 2335. (e) Kajzar, F.; Etemad, S.; Baker, G. L.; Messier, J. *Synth. Met.* **1987**, *17*, 563.

(8) (a) Davydov, A. S. *Solitons in Molecular Systems;* Kluwer-Reidel: Dordrecht, The Netherlands, 1995. (b) *Handbook of Conducting Polymers*; Skotheim, T. A., Elsenbaumer, R. L., Reynolds, J. R., Eds.; Marcel Dekker: New York−Basel−Hong Kong, 1998. (c) *Relaxation in Polymers*; Kobayashi, T., Ed.; World Scientific: Singapore, 1993.

(9) (a) Roth, S.; Bleier, H. *Adv. Phys.* **1987**, *36*, 385. (b) Heeger, A. J.; Kivelson, S.; Schrieffer, J. R.; Su, W.-P. *Rev. Mod. Phys.* **1988**, *60*, 781−850. (c) Vardeny, Z. V.; Wei, X. In *Handbook of Conducting Polymers*; Skotheim, T. A., Elsenbaumer, R. L., Reynolds, J. R., Eds.; Marcel Dekker: New York−Basel−Hong Kong, 1998, pp 639−666. (d) Orenstein, J. In *Handbook of Conducting Polymers*; Skotheim, T. A., Ed.; Marcel Dekker: New York−Basel, 1986; Vol. 2, p 1297. (e) Pople, J. A.; Walmsley, S. H. *Mol. Phys.* **1962**, *5*, 15. (f) Reid, R. D.; Schug, J. C.; Lilly, A. C.; Dwyer, R. W. *J. Chem. Phys.* **1988**, *88*, 2049. (g) Chien, F.; Kashimori, Y.; Nishimoto, K.; Tanimoto, O. *Chem. Phys.* **1988**, *125*, 269. (h) Kobayashi, T. *Synth. Met.* **1995**, *71*, 1663. (i) Block, S.; Streitwolf, H. W. *Synth. Met.* **1996**, *76*, 31. (j) Groves, M. P.; Carvalho, C. F.; Prager, R. H. *Mater. Sci. Eng., C* **1995**, *3*, 181. (k) Rubner, O.; Förner, W.; Ladik, J. *Synth. Met.* **1993**, *61*, 279. (l) Förner, W. *Adv. Quantum Chem.* **1994**, *25*, 207. (m) Flood, J. D.; Heeger, A. *J. Phys. Rev. B* **1983**, *28*, 2356. (n) Moraes, F.; Park, Y. W.; Heeger, A. J. *Synth. Met.* **1986**, *13*, 113. (o) Rothberg, L.; Jedju, T. M.; Etemad, S.; Baker, G. L. *Phys. Rev. Lett.* **1986**, *57*, 3229. (p) Rothberg, L.; Jedju, T. M. *Phys. Rev. Lett.* **1990**, *65*, 100. (q) Ehrenfreund, E.; Moses, D.; Hegger, A. J.; Cornil, J.; Bredas, J. L. *Chem. Phys. Lett.* **1992**, *196*, 84. (u) Bauerlr, P.; Segelbacher, U.; Gaudl, K.-U.; Huttenlocher, D.; Mehring, M. *Angew. Chem., Int. Ed. Engl.* **1993**, *32*, 76. (s) Zotti, G.; Schiavon, G.; Berlin, A.; Pagani G. *Chem. Mater.* **1993**, *5*, 620.

Chart 3

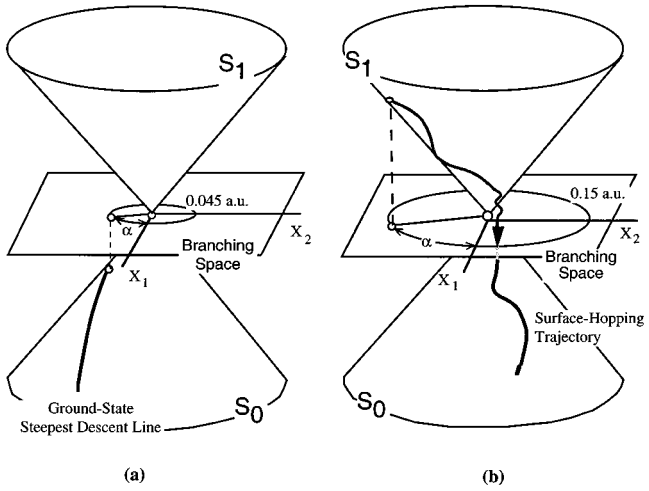

2. Computational Details

A variety of methods have been used for the present investigation, including MEP computations[2,10] and semiclassical trajectory simulations.[6] CAS−SCF energy and gradient computations have been carried out on the short-chain polyene systems (the "central" bond *cis-tZt*-C_6H_8 and the *all-trans*-C_8H_{10}) with a complete active space (CAS) using the 6-31G* basis set available in Gaussian 94.[4b] The choice of active space in our computations is unambiguous and consists of all the electrons and orbitals which form the π-system in the polyenes.

The S_0 MEP from the conical intersection region has been determined using a method[10] for the location of the initial direction of relaxation (IRD)[10b] from the starting point (the conical intersection). Once the IRD has been determined, the MEP is computed as the steepest descent line in mass-weighted Cartesians, using the IRD vector to define the initial direction to follow. In a manner analogous to the MEP for thermal reactions, this steepest descent path provides a "structural" (i.e. for infinitely slow motion) nondynamical description of the relaxation process.

When the MM−VB potential is used, the position of the S_0 relaxation valleys originating at the conical intersection is evaluated using a slightly different method based upon the computation of a set of steepest descent lines (SDLs) in mass-weighted Cartesians. These lines start at points located on the conical intersection branching space, which is given by a plane defined by the gradient difference ($\mathbf{X}_1$) and nonadiabatic coupling ($\mathbf{X}_2$) vectors. These are the only two molecular displacement vectors (out of $3N - 6$) that can lift the S_1/S_0 energy degeneracy. Chart 3 shows that when the S_1 and S_0 energies are plotted along the branching plane, they form a double cone.[1e] Typically the SDLs are started from points evenly distributed along a small circle centered at the apex of the cone (radius 0.045 amu$^{1/2}$ bohr). One of these steepest descent lines is illustrated in Chart 3a. The "width" of the valley (the SDL catchment region) is given by a many-to-one correlation between the starting angles and the common point where a group of SDLs terminates.

Ab initio CAS−SCF dynamics simulations through a conical intersection point are too expensive to be used routinely (see ref 11 for an example of ab initio dynamics on a system with three conjugated double bonds). Thus, the semiclassical dynamics computations have been carried out using a trajectory-surface-hopping (TSH) method with a hybrid MM−VB force field to model the ab initio potentials (details can be found elsewhere[5]). Trajectories have been computed starting with the excited $2A_g$ (S_1) state from a "circle" of points (radius 0.15 amu$^{1/2}$ bohr) in the branching space around the conical intersection, with the initial kinetic energy distributed in randomly sampled vibrational modes. One of these semiclassical trajectories is illustrated in Chart 3b.

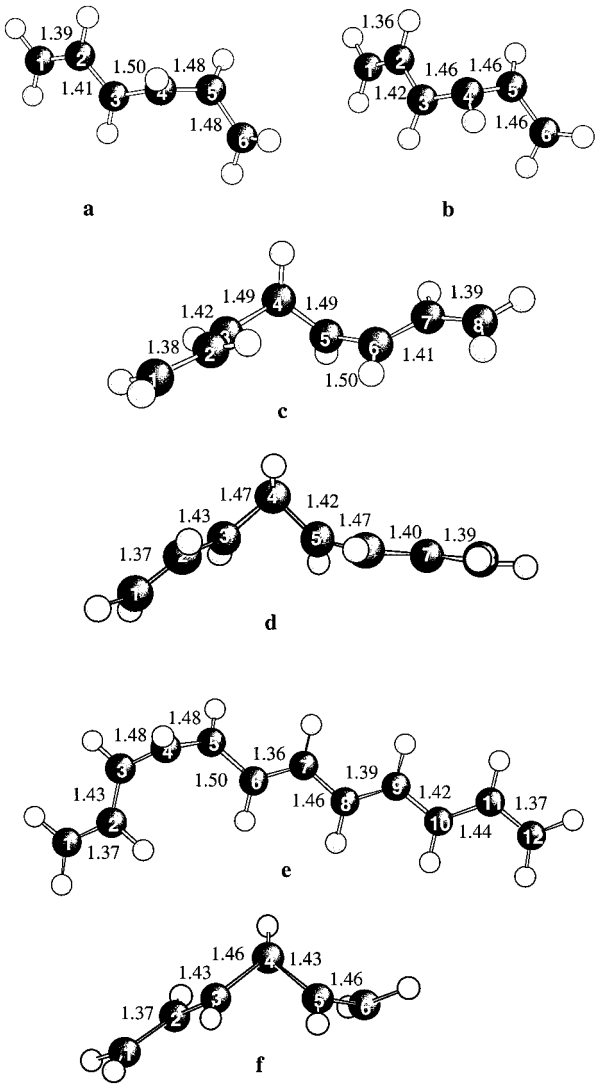

Figure 1. (a) MM−VB-optimized conical intersection geometry for *tZt*-C_6H_8. (b) CAS−SCF-optimized conical intersection geometry for *all-trans*-C_6H_8. (c) MM−VB-optimized conical intersection geometry for *all-trans*-C_8H_{10}. (d) CAS−SCF-optimized conical intersection geometry for *all-trans* C_8H_{10}.[13b] (e) MM−VB-optimized conical intersection geometry for *all-trans*-$C_{12}H_{14}$. (f) CAS−SCF-optimized conical intersection geometry for *all-trans*-C_6H_8.[1c] All bond lengths are in angstroms.

For the dynamics simulations to be meaningful, we must demonstrate that the $3N - 6$ dimensional MM−VB potential reproduces the important features of the ab initio surface in the region of the conical intersection (i.e., that the geometry and energetics of the MM−VB-optimized relevant structures and MEP are in agreement (at least qualitatively) with the available corresponding ab initio data). Qualitative agreement between CAS−SCF and MM−VB potential energy surfaces has already been demonstrated in several conjugated systems.[10b,12] In parts a and b and parts c and d, respectively, of Figure 1 we show the CAS−SCF- and MM−VB-optimized conical intersection geometries for *tZt*-C_6H_8 and *all-trans*-C_8H_{10}. The main geometrical parameters (including the $C_3-C_4-C_5$ kink at the conical intersection) are reproduced by MM−VB results, apart from the pyramidalization at C_4, which has a negligible energetic effect. Moreover, as we shall discuss subsequently, the inverted π-electron coupling region on the S_0 potential energy surface can be represented at the CAS−SCF and MM−VB levels of theory, with all the main geometrical and electronic features being in good agreement.

(10) (a) Celani, P.; Robb, M. A.; Garavelli, M. Bernardi, F.; Olivucci, M. *Chem. Phys. Lett.* **1995**, *243*, 1. (b) Garavelli, M.; Celani. P.; Fato, M.; Bearpark, M. J.; Smith, B. R.; Olivucci, M.; Robb, M. A. *J. Phys. Chem. A* **1997**, *101*, 2023.

(11) Vreven, T.; Bernardi, F.; Garavelli, M.; Olivucci, M.; Robb, M. A. Schlegel, H. B. *J. Am. Chem. Soc.* **1997**, *119*, 12687−12688.

(12) (a) Bearpark, M. J.; Bernardi, F.; Olivucci, M.; Robb, M. A. *Chem. Phys. Lett.* **1994**, *217*, 513. (b) Bearpark, M. J.; Bernardi, F.; Olivucci, M.; Robb, M. A. *J. Phys. Chem. A* **1997**, *101*, 8395.

The data from our trajectory computations will be displayed via snapshots of geometries from some of the most representative computed trajectories and by plotting structural data, such as bond lengths. However, the assignment of double versus single bonds can be ambiguous because of large amplitude vibrations. Thus, we have also documented the changes in bonding along the computed S_0 paths using concepts derived from VB theory.[13] An indication of the double versus single bond nature can be obtained by plotting the spin exchange density, P_{ij}, for each pair of carbon atoms (see ref 14d for a more detailed discussion on exchange density matrix elements P_{ij}).

In the valence bond approach, the energy may be expressed in terms of an "exchange density matrix", P_{ij}, and is defined as

$$E = Q + \sum_{ij} P_{ij} K_{ij}$$

where Q is the coulomb energy and the exchange integral K_{ij} is negative as in the Heitler−London VB problem for all bonded $i-j$ pairs. The values of the matrix elements P_{ij} provide concise information about the spin coupling of the VB wave function. A P_{ij} value of $+1$ corresponds to a situation where electrons in orbitals i and j are paired (singlet spin coupled or bonded). In contrast, a value between 0 and -1 indicates that the centers are either uncoupled (a value of $-1/2$ corresponds to electrons which are nonbonded) or triplet spin coupled (-1 or antibonding). During a trajectory with electronic rearrangements one can expect to see all values between these two limits. For example, in a trajectory with considerable excess vibrational energy one may see long bond lengths (>1.5 Å) but with an associated P_{ij} value corresponding to double bond character. This is because the momentum in the vibration present may cause the geometry to "lag behind" electronic change as measured by the P_{ij} value. Thus, rather than simply looking at the bond lengths in a molecule as a function of time (which are merely "reacting" to changes in P_{ij}), a more fundamental view of the bonding as a function of time is given by the P_{ij} values themselves (such an approach was taken, for example, in ref 14b). Thus, exchange density (P_{ij}) data are used to examine the change in bonding and investigate the driving force behind the effect.

3. Results and Discussion

The relaxation process which follows decay at the conical intersection must be initiated via a molecular deformation in the subspace of the branching plane ($\mathbf{X}_1$, $\mathbf{X}_2$). Inspection of the $\mathbf{X}_1$ and $\mathbf{X}_2$ vectors for the $-(CH)_3-$ kink (the $\mathbf{X}_1$ and $\mathbf{X}_2$ vectors of *all-trans*-C_8H_{10} are given in the Chart 4) suggests that motion mainly along the $\mathbf{X}_1$ vector but with some component of $\mathbf{X}_2$ leads to formation of a closed-shell polyene, initiated by double bond formation at C_5-C_6. However, motion along the reverse direction $-\mathbf{X}_1$ leads toward a π-diradical structure, since the double bond is formed at the position C_4-C_5, which leaves two π-electrons unpaired. Thus, these deformations induce specific

Chart 4

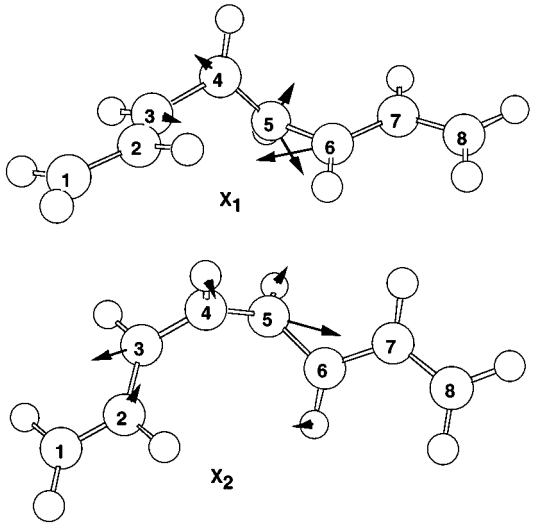

electron pairing in the four weakly interacting electrons of the kink electronic structure. Accordingly, the formation of π-diradical species is an intrinsic property of the electronic structure of polyene conical intersections.

We shall provide evidence that radiationless deactivation of the $2A_g$ of a polyene in the vicinity of a conical intersection of the "$-(CH)_3-$ kink" type can indeed trigger the formation of a π-diradical species with a finite lifetime. To do that, in section 3.1 we use ab initio CAS−SCF MEP computations[14,19] to locate the ground-state relaxation valleys for C_6H_8, while for the longer polyenes C_8H_{10} and $C_{12}H_{14}$ we use MM−VB SDL calculations. We will show that the existence of a relaxation path involving species with single bond/double bond inversion and diradical character is a general feature in both short and longer polyenes. In section 3.2 we present the investigation of the deactivation dynamics of the longer polyene $C_{12}H_{14}$ using semiclassical trajectory computations. These results show that a transient π-diradical species with single bond/double bond inversion can be generated ca. 40 fs after decay of the excited state and could live long enough to be observed experimentally.

3.1. Inverted π-Electron Coupling in Linear Polyenes. We begin with a discussion of the computed ground-state relaxation MEP departing from the conical intersection of *tZt*-C_6H_8 (see Figure 1b). Notice that in this case the $-(CH)_3-$ kink is located at the central $C_3-C_4-C_5$ segment (similar ab initio studies have been performed for *all-trans* (*tEt*) hexatriene[1c] and *all-trans* (*tEtEt*) octatetraene[1b] with the same conclusions; see section S.1 in the Supporting Information). A ground-state small-radius hypersphere search (see section 2 and ref 10 for details) around the conical intersection yields two different initial relaxation

(13) (a) The simplest example of a three-center conical intersection occurs in the H_3 system, $H + H_2 \rightarrow H_2 + H$. Taking the potential energy expression to be $E = Q \pm K$ (see: McWeeny, R.; Sutcliffe, B. T. *Methods of Molecular Quantum Mechanics*; Academic Press: New York, 1969. Eyring, H.; Walter, J.; Kimball, G. *Quantum Chemistry*; Wiley: New York, 1944), the exchange component K vanishes when all three H−H distances are equal—i.e., when the atoms form an equilateral triangle. In these points the D_0 (ground) and D_1 (excited) states are then degenerate, defining the conical intersection hyperline. At any point on the hyperline, all three electrons are uncoupled, and are not associated with any H−H bond. After decay through the conical intersection, any of the three equivalent couplings can occur. This simple example is surprisingly useful for predicting and interpreting more complex systems.

(14) (a) Bernardi, F.; Celani, P.; Olivucci, M.; Robb, M. A.; Suzzi-Valli, G. *J. Am. Chem. Soc.* **1995**, *117*, 10531−10536. (b) Bearpark, M. J.; Bernardi, F.; Olivucci, M.; Robb, M. A. *Int. J. Quantum Chem.* **1996**, *60*, 505−512. (c) Bearpark, M. J.; Bernardi, F.; Olivucci, M.; Robb, M. A.; Smith, B. R. *J. Am. Chem. Soc.* **1996**, *118*, 5254−5260. (d) Bearpark, M. J.; Robb, M.A.; Bernardi, F.; Olivucci M. *Chem. Phys. Lett.* **1994** *217* 513−519. (e) Pauncz, R. *Spin Eigenfunctions*; Plenum Press: New York, 1979. (f) Bernardi, F.; Olivucci, M.; McDouall, J. J. W.; Robb, M. A. *J. Chem. Phys.* **1988**, 89, 6365−6375.

(15) For dodecahexaene it is quite simple to locate a conical intersection with the kink at other positions in the molecule. Moving the kink has little effect on the energetics of the conical intersection; optimizing with the kink at $C_5-C_6-C_7$ (i.e., more toward the middle of the chain) lowers the energy by only ~1.5 kcal/mol compared to the structure with the kink at $C_3-C_4-C_5$. However, for our purposes we keep the kink in the same position as for the other polyenes.

(16) (a) Vardeny, Z. V.; Wei, X. *Synth. Met.* **1993**, *54*, 99. (b) Wei, X.; Hess, B. C.; Vardeny, Z. V. *Phys. Rev. Lett.* **1992**, *68*, 666. (c) Kivelson, S.; Wu, W.-K. *Phys. Rev.* **1986**, *34*, 5423. (d) Levey, C. G.; Lang, D. V.; Etemad, S.; Baker, G. L.; Orenstein, J. *Synth. Met.* **1987**, *17*, 569.

(17) Das, G. P.; Yeates, A. T.; Dudis, D. S. *Int. J. Quantum Chem.* **1996**, *60*, 287. (b) Das, G. P.; Yeates, A. T. *Int. J. Quantum Chem.* **1996**, *59*, 251.

(18) (a) Su, W.-P. *Phys. Rev. B* **1986**, *34*, 2988. (b) Su, W.-P. *Phys. Rev. B* **1987**, *36*, 6040.

(19) Tavan, P.; Schulten, K. *Phys. Rev.* **1987**, *36*, 4337.

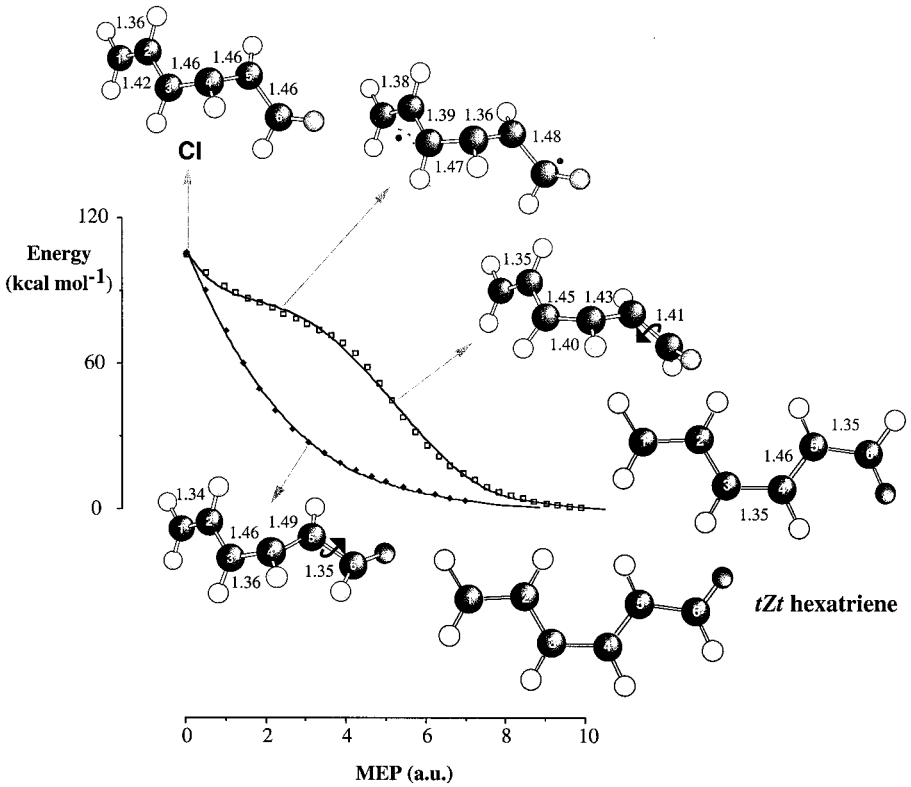

Figure 2. *tZt*-C_6H_8 energy profiles along the computed ab initio MEP describing the relaxation from the S_1/S_0 (i.e., $-(CH)_3-$ kink) conical intersection (CI) to the final photoproduct (*tZt*-hexatriene). The terminal hydrogen atom in the structures has been marked in black to indicate the stereochemistry. Bond lengths are in angstroms.

directions, from which two qualitatively different MEPs have been located (see Figure 2). The first MEP (full diamonds) leads directly back to the *tZt*-C_6H_8 equilibrium structure and is characterized by a rapid decrease in energy. The molecular structure located halfway along the MEP indicates that the original closed-shell bond alternation is rapidly recovered. On the other hand, while the second MEP (open squares) shows a barrierless energy profile leading to the same equilibrium structure, the initial part contains an inflection point (i.e., a shoulder). At the shoulder, the geometrical and electronic structures of the molecule are consistent with the presence of a double bond/single bond inversion, which we can denote as $(C_1-C_2-C_3)^{\bullet}-(C_4=C_5)-(C_6)^{\bullet}$. One can observe that the bond alternation occurring along the $C_3-C_4-C_5$ fragment is exactly opposite the one seen in the first MEP. In other words, the second (higher energy) MEP shows a region with inverted π-electron coupling sandwiched between two radical centers, $(C_1-C_2-C_3)^{\bullet}$ and $-(C_6)^{\bullet}$. This π-diradical subsequently evolves toward the more stable closed-shell polyene, through the rotation of the twisted terminal methylene. The values of the bond lengths along the inverted coupling region of the MEP are plotted in Figure 3 together with "snapshots" of selected geometries along the MEP. By step 5, the inverted coupling is clearly established (the C_4-C_5 bond length is 1.36 Å). The normal coupling is restored by step 14, and is accompanied by a terminal C−C twisting deformation. The relative stability of the π-diradical must depend on the chain length. We now document this effect by computing the minimum energy paths for *tZt*-C_6H_8, *all-trans*-C_8H_{10}, and *all-trans*-$C_{12}H_{14}$ using MM−VB. The results demonstrate that the π-diradical region located along the MEP becomes flat and corresponds to a high-energy plateau in longer polyenes.

Following the procedure described elsewhere,[10b] we have probed the ground-state relaxation paths from the tip of the conical intersections (shown in Figure 1a,c,e) by computing a series of MM−VB steepest descent lines starting from a circle centered on the apex of the cone (see section 2 and Chart 3a for the details). Remarkably, these lines do not always terminate at a closed-shell structure, but rather, the MEP "stalls" at regions located along a high-energy plateau on the S_0 potential energy surface, where the gradient is near zero. Full geometry optimization in the domain of this plateau is impractical because the potential surface is very flat. The approximately optimized MM−VB structures centered on three MEPs are collected in Figure 4.

Ground-state structures featuring inverted coupling for C_8H_{10} (Figure 4b) and for $C_{12}H_{14}$ (Figure 4c) have geometrical features similar to the "shoulders" seen in the CAS−SCF MEP of Figure 2 and the MM−VB MEP of Figure 4a (*all-trans*-hexatriene). Notice that in C_6H_8 the two shoulder structures—the second ab initio structure in Figure 2 and the MM−VB structure of Figure 4a—are similar and demonstrate that the MM−VB method is capable of providing a good approximation of the much more expensive ab initio CAS−SCF method.

There are two striking features of the π-diradical structures in Figure 4. First, for *all-trans*-octatetraene, the single bond/double bond alternation of the three central C−C bonds is inverted, with a fully formed double bond between atoms C_4 and C_5 corresponding to $(C_1-C_2-C_3)^{\bullet}-(C_4=C_5)-(C_6-C_7-C_8)^{\bullet}$. Second, the unpaired electrons are not isolated on the terminal carbon atoms but are delocalized on allyl-like moieties, $(C_1-C_2-C_3)^{\bullet}$ and $(C_6-C_7-C_8)^{\bullet}$ at each end of the molecule. Apart from this second feature, the structures are similar to that of the π-diradical species schematically represented in section 1 (structure 3). As discussed previously, the reversal of bond alternation must necessarily generate two unpaired electrons on either side of the kink deformation, and the stabilization of this species by the allyl moieties can be rationalized in terms of

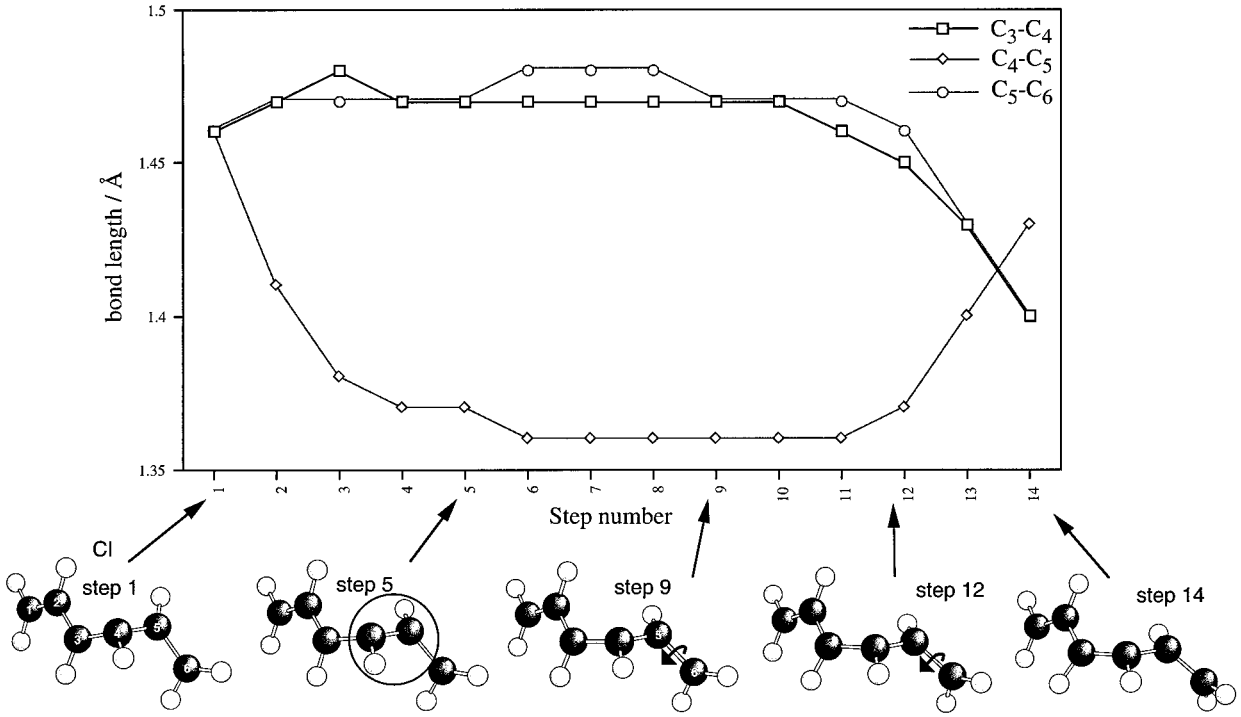

Figure 3. Ab initio evidence for inverted π-electron coupling in *tZt*-C_6H_8. The graph shows three C−C bond lengths (in angstroms) for each step of the ground-state MEP, beginning at a point near the conical intersection.

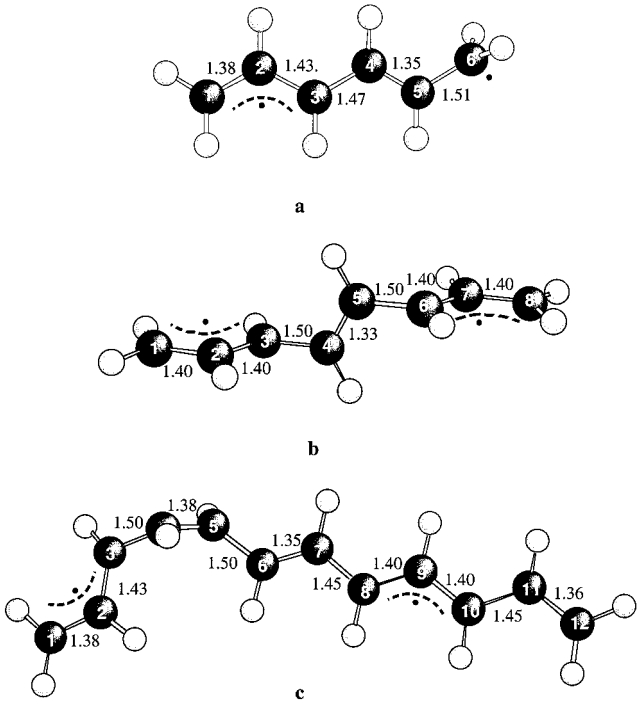

Figure 4. (a) MM−VB ground-state inverted π-electron coupling geometry for *all-trans*-C_6H_8 (not fully optimized). (b) MM−VB-optimized ground state at the inverted π-electron coupling minimum for *all-trans*-C_8H_{10}. (c) MM−VB-optimized ground-state inverted π-electron coupling geometry for *all-trans*-$C_{12}H_{14}$ (not fully optimized).

resonance structures. Except for some torsional angles, the ground-state π-diradical structure for *all-trans*-hexatriene (Figure 4a) displays the same geometric and electronic features.

The longer dodecahexaene ($C_{12}H_{14}$) chain can be considered as a "minimal" polyacetylene model.[15] Thus, it is instructive to examine the path leading to the inverted coupling region in more detail in this case. (See the Supporting Information, section 5.2 for details.) Figure 5 shows one of the inverted coupling paths computed for *all-trans*-$C_{12}H_{14}$. The seven central C−C bond lengths are plotted at each step, together with some snapshots of the molecular geometry. The result is qualitatively similar to the ab initio MEP for *tZt*-C_6H_8 (Figure 2). By step 100 there is an almost fully formed double bond at C_4C_5 (as well as at C_6C_7), the $-C_4HC_5H-$ segment becomes planar, and the structure is similar to that shown in Figure 4c. At step 150, in a manner similar to that of the ab initio results for *tZt*-C_6H_8 (Figure 2), the coupling starts to reverse, restoring double bonds at C_3C_4 and C_5C_6. The corresponding $-C_3HC_4H-$ and $-C_5HC_6H-$ segments become planar. Note that all the C−C bond lengths react simultaneously with the deformation at the kink, although sites further from the kink are affected least. The C−C bonds at the head and tail of the chain (not plotted) are largely unaffected by the change of coupling at the kink, and so these retain double bond character throughout.

3.2. π-Diradical Creation and Annihilation Dynamics. Following a strategy reported elsewhere[10b] and briefly summarized in section 2, we have carried out semiclassical trajectory computations starting from a series of excited-state points evenly distributed along a circle centered on the tip of the conical intersection and lying in the corresponding branching space. The analysis of the trajectories provides information on the mechanism and time scale of formation and annihilation of the π-diradicals seen in Figure 4. (See section S.3 in the Supporting Information for further details.)

For the current analysis, we define the lifetime of the π-diradical as the amount of time spent in the ground state, during which the inverted coupling is present within the ($C_3-C_4-C_5$) fragment and before annihilation through return to the standard double bond/single bond alternation. The results in Table 1 show the computed lifetimes for the π-diradical species for the three polyenes under investigation. These data are obtained from a sample of 64 trajectories which enter the inverted coupling region. The maximum lifetimes are remarkably high. From Table 1, one can see that the longest chain, $C_{12}H_{14}$, can retain the inverted coupling for up to ~1 ps. The

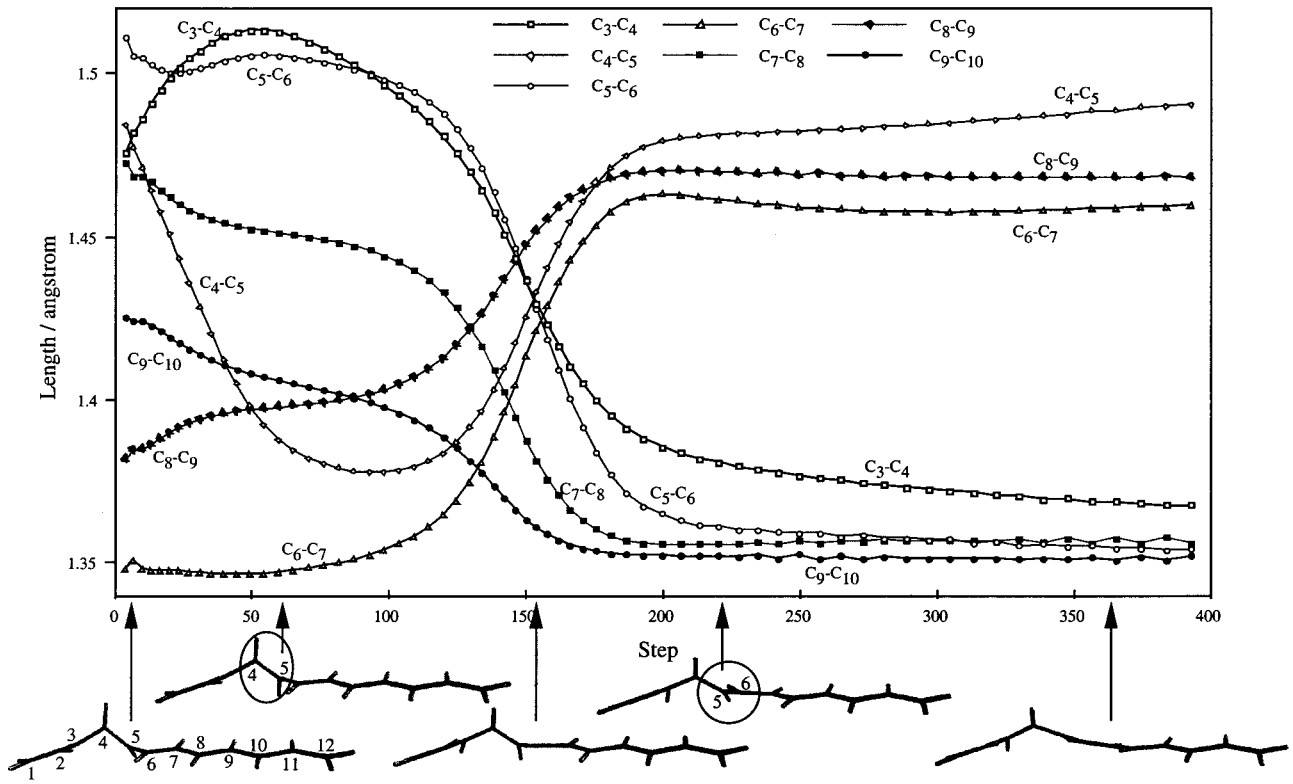

Figure 5. Main bond lengths and geometries for an MEP toward the inverted π-electron coupling region in $C_{12}H_{14}$.

Table 1. Time (fs) Taken for the Normal π-Electronic Coupling To Be Restored[a]

	C_6H_8	C_8H_{10}	$C_{12}H_{14}$
min	18.1	52.1	33.3
max	105.0	239.4	961.1
mean	70.1	118.1	136.6
std dev	23.5	63.7	174.1

[a] Data obtained by analyzing three batches of excited-state trajectories; see the text (and section S.3 in the Supporting Information) for details.

analysis of the trajectories reveals that the $C_{12}H_{14}$ chain undergoes a quasi-periodic motion which keeps the molecule within the π-diradical energy plateau. Since the decay path computation of section 3.1 shows that there is no well-defined potential energy valley to hold the trajectories in this region, it appears that the trajectories are "dynamically locked" in certain vibrational modes.

To illustrate this dynamic locking, in Figure 6 we plot the C_4-C_5 and C_5-C_6 bond lengths along two typical $C_{12}H_{14}$ trajectories. After moving into the plateau region (upper left of the figure), where one has a short C_4-C_5 bond and a long C_5-C_6 bond, one trajectory (faint line in Figure 6) returns to the normal coupling (lower right of the figure) after only a couple of oscillations. In contrast, the other trajectory (bold line in Figure 6) performs many oscillations in the π-diradical region, and the molecule does not undergo electron recoupling within the time period plotted and remains dynamically confined. A geometry optimization starting from any point along the confined trajectory would eventually lead to the energy well corresponding to the original ground-state reactant or to one of its cis or trans isomers. Comparison of the electronic structure of the transient π-diradical species, with the $-(CH)_3-$ kink at the excited-state decay point, suggests that, in our simulation, the probability of formation of a polyene segment with an inverted π-electron coupling is obviously related to the electronic

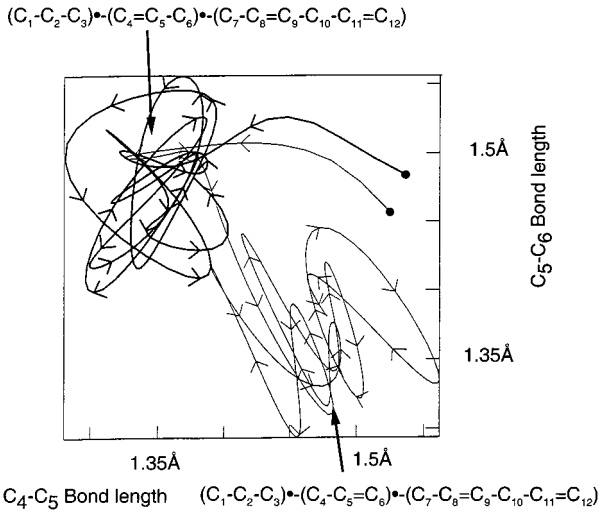

Figure 6. 4−5 and 5−6 bond lengths for two randomly selected $C_{12}H_{14}$ trajectories.

structure of the decay channel and to the initial conditions (i.e., the initial position on the S_1 energy surface and the initial momentum; see also section S.3 in the Supporting Information).

Within our simulation, which starts at points evenly distributed about the intersection point and randomly distributed kinetic energies (see section 2), we now document the existence of three types of trajectories, which provide examples of the different mechanisms for the S_0 relaxation of the photoexcited polyene chain. In the following discussion, it is convenient to use a simple scheme for indicating the structures and electron couplings. Thus, we will use the notation $(C_1-C_2-\mathbf{C_3})^{\bullet}-(\mathbf{C_4}^{\bullet}-\mathbf{C_5}^{\bullet})-(C_6-C_7-C_8-C_9-C_{10}-C_{11}-C_{12})^{\bullet}$ to denote the conical intersection, where the position of the original $-(CH)_3-$ kink is indicated in bold.

The first type of trajectory (type i) is characterized by direct relaxation (i.e., fast relaxation to the closed-shell pattern of single

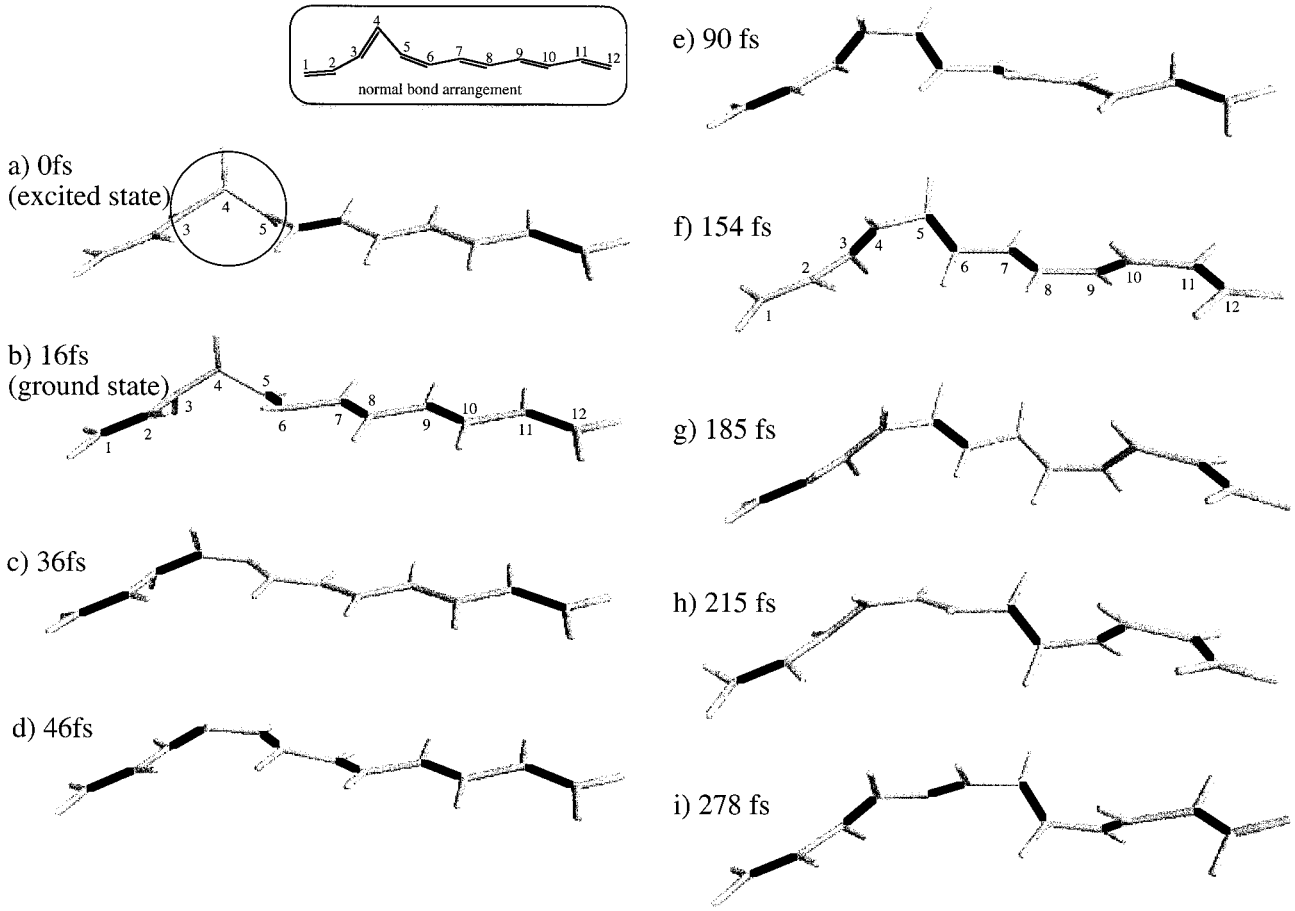

Figure 7. Snapshots from a $C_{12}H_{14}$ trajectory started near the conical intersection on the excited-state S_1 surface (geometry a), following the "normal" π-electron coupling path. Bond lengths of less than 1.37 Å are indicated in bold.

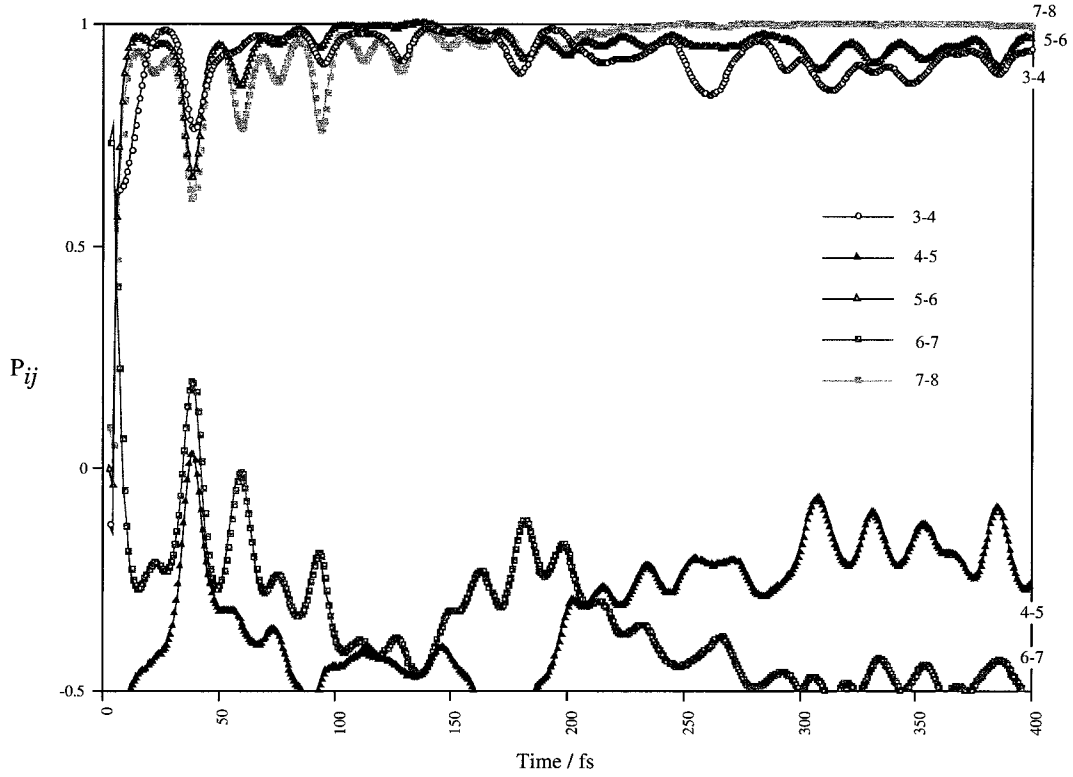

Figure 8. Exchange density data (P_{ij}) for a normal π-electron coupling trajectory.

and double bonds; see Figures 7 and 8). In this case the geometrical distortion, which corresponds to the $-(CH)_3-$ kink, disappears immediately. At the same time recoupling of the radical centers on C_3/C_4 and C_5/C_6 leads to double bond formation to give the (C_1═C_2–**C_3═C_4**)–(**C_5**═C_6–C_7═C_8–C_9═C_{10}–C_{11}═C_{12}) pattern, i.e., the normal closed-shell struc-

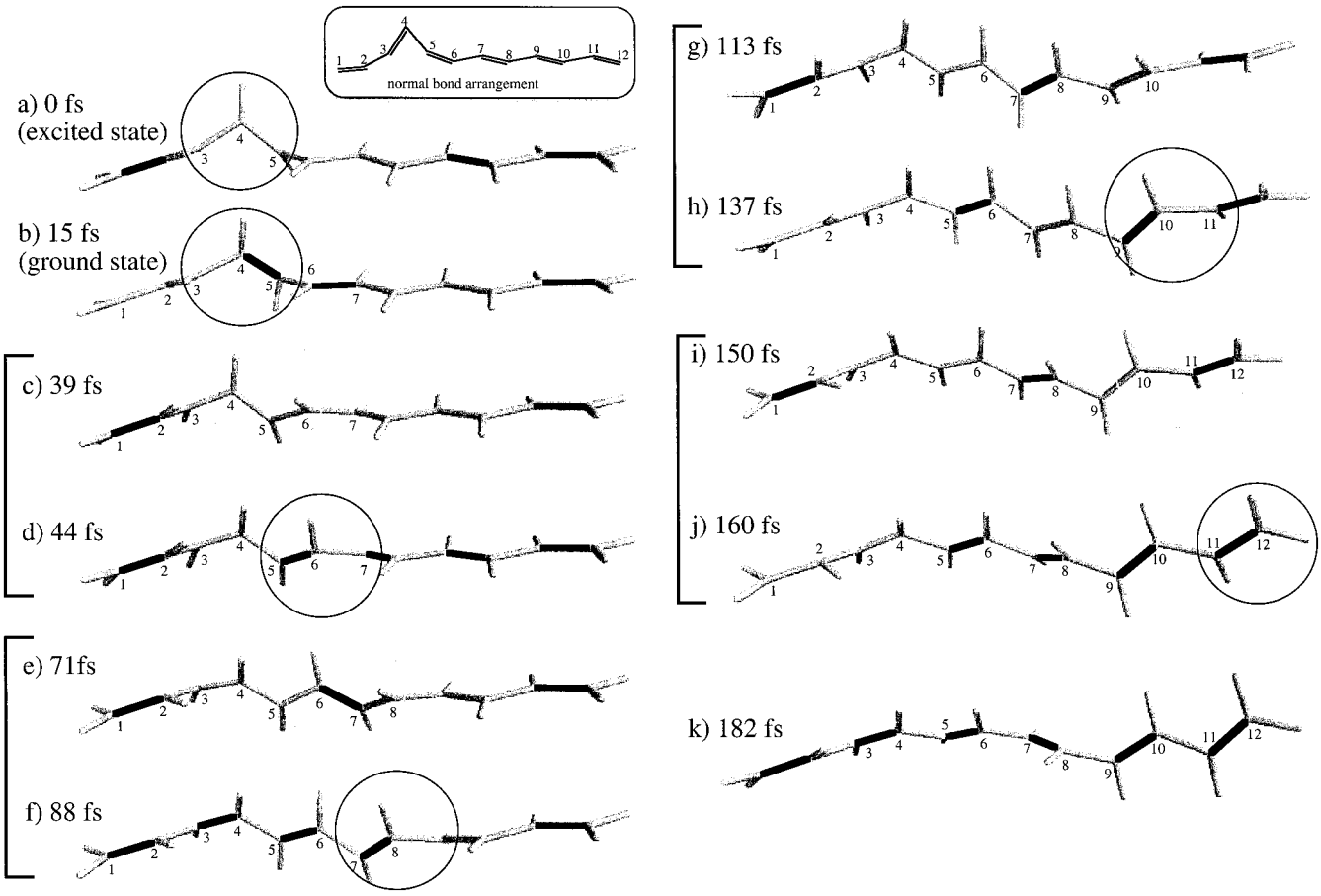

Figure 9. Snapshots from a $C_{12}H_{14}$ trajectory started near the CI on the excited-state surface, with a short inverted π-electron coupling lifetime. Bond lengths of less than 1.37 Å are indicated in bold. The kink is circled at each frame. The faint circles are the "transitional" kink structures, discussed in the text.

ture. The second and third types of trajectories (types ii and iii) are characterized by a change of the $-(CH)_3-$ kink shape which persists after the initial relaxation. In these trajectories the electron recoupling process is initially inverted, yielding a C_4C_5 double bond and two radical moieties on $(C_1-C_2-C_3)^{\bullet}$ and $(C_6-C_7-C_8-C_9-C_{10}-C_{11}-C_{12})^{\bullet}$. These two types of trajectories differ in both the lifetime and annihilation mechanism of the π-diradical state. As we will describe in more detail below, the lifetime of this transient varies in different trajectories from a few tens of femtoseconds to over 1 ps (see Table 1). In the trajectories of type ii the initially formed π-diradical has a short lifetime and undergoes a ca. 40 fs electron recoupling process that leads to the conventional double bond patterns $(C_1{=}C_2-\mathbf{C_3{=}C_4})-(\mathbf{C_5{=}}C_6-C_7{=}C_8-C_9{=}C_{10}-C_{11}{=}C_{12}$. In contrast, in the trajectories of type iii, the inverted coupling pattern of the π-diradical persists for a much longer time (160 fs in the example discussed below). Trajectories of types ii and iii (shown as light and bold lines in Figure 6, respectively) correspond to the two different lifetimes of the inverted coupling.

Remarkably the results of our simulations show that the π-diradical annihilation process is always characterized by the propagation of a kink (an out-of-plane distortion of the polyene chain) along the polyene chain which originates at the original $-(CH)_3-$ conical intersection structure. Below, we show that in the type ii case the kink only propagates along a polyene chain characterized by closed-shell bond ordering (see Figures 9−12) while, in the type iii case, the kink propagates along a chain with inverted bond ordering (Figures 13 and 14).

Each case has been analyzed by plotting a set of trajectory snapshots. Each snapshot has been characterized by marking the bonds which are less than 1.37 Å (i.e., those with double bond character) in bold and circling the position of the kink at each frame. Furthermore, the changes in the bonding of the corresponding molecular arrangement have been quantified by computing the P_{ij} exchange density matrix elements. (See the Computational Details for a discussion.) Plots of these parameters as a function of time give a simple picture of the electronic driving force for the trajectory.

We begin with a discussion of the trajectories of type i which lead to direct relaxation to the closed-shell polyene. In Figure 7 we show the structures as a function of time, and in Figure 8 we report the corresponding P_{ij} values. The recoupling of the radical centers on C_3-C_4 and C_5-C_6 leading to the normal ordering of single and double bonds to give $(C_1{=}C_2-C_3{=}C_4)-(C_5{=}C_6-C_7{=}C_8-C_9{=}C_{10}-C_{11}{=}C_{12})$ is complete within 36 fs (see structure c of Figure 7). The structure then relaxes through C_3-C_4 and C_5-C_6 torsions, to stabilize the double bond formation, thus yielding a ground-state polyene. From Figure 8, it can be seen that the expected "normal" values of the P_{ij} for single and double bonds are also established within 50 fs.

Now let us consider the trajectories of type ii, where the relaxation process involves the initial formation of a short-lived π-diradical and is followed by the propagation of the kink along a polyene chain with closed-shell π-electron coupling. Figures 9 and 10 depict a series of snapshots for this trajectory, starting with the excited-state surface near the conical intersection. Bond lengths of less than 1.37 Å are highlighted in bold. The $-(CH)_3-$ kink is circled at each frame. To accompany the snapshots, in Figure 11, we also plot the C_3-C_4, C_4-C_5, and C_5-C_6 bond lengths as functions of time. Structure a (Figures

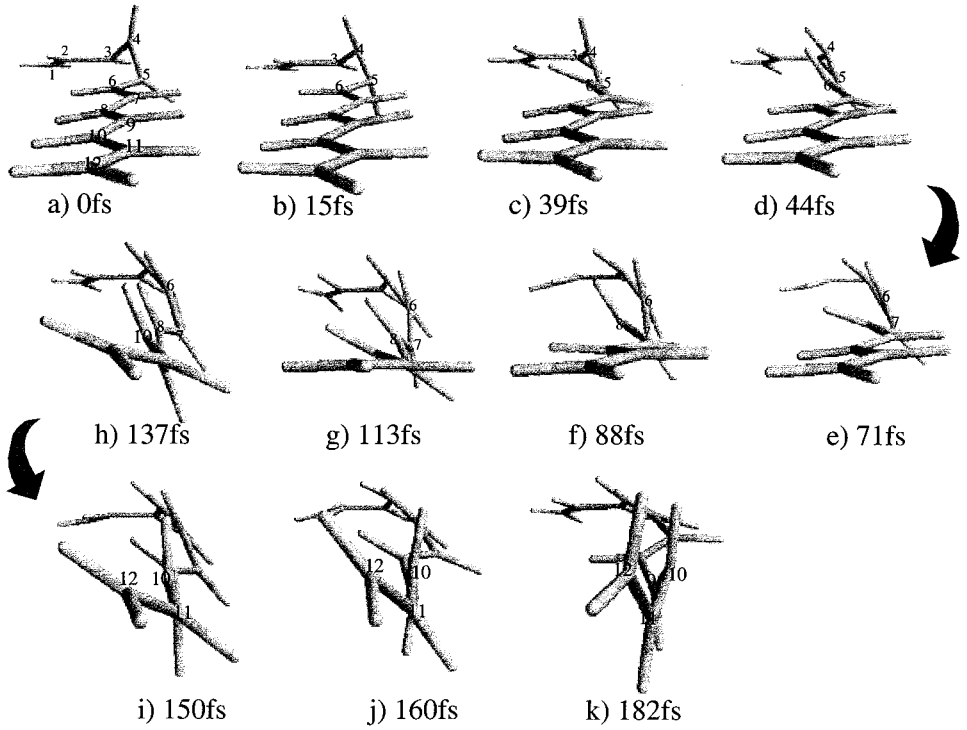

Figure 10. Snapshots from the same trajectory as in Figure 9, but viewed from the end of the chain.

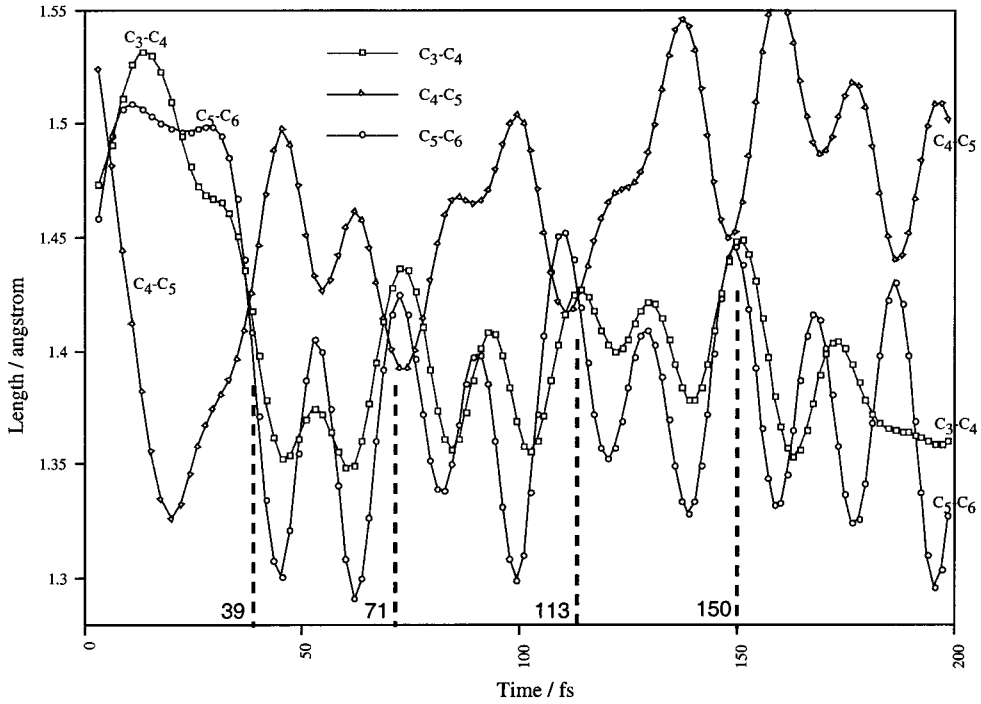

Figure 11. Main bond lengths for the trajectory shown in Figures 9 and 10.

9 and 10) is the initial S_1 geometry (close to the conical intersection point). After 15 fs, the inverted coupling is established, making double bonds at C_4-C_5 and C_6-C_7 (structure b), which we denote $(C_1-C_2-\mathbf{C_3})^{\bullet}-(\mathbf{C_4}=\mathbf{C_5})-(C_6=C_7-C_8-C_9-C_{10}-C_{11}-C_{12})^{\bullet}$. The bond length plot (Figure 11) clearly shows that these are formed *simultaneously*. The geometry at 15 fs is almost identical to the "optimized" inverted coupling structure of Figure 4c. (As mentioned above, the inverse coupling status is not stable along trajectories of type ii). At ~39 fs the geometry of the molecule passes through a curious vibration where none of the central C−C bonds are short, and the plot of bond length versus time shows all lines passing through almost the same point (~1.42 Å). This is not a spurious occurrence, but is common to all trajectories of this type. As indicated by the vertical dashed lines in Figure 11, analogous structures are generated later in the simulation after almost constant time intervals of ca. 40 fs. At the first 39 fs point (structure c in Figures 9 and 10) the $C_4-C_5-C_6$ moiety becomes allylic (see also Figure 9) and the corresponding $-(CH)_3-$ unit becomes planar. At this stage the kink (in bold) moves forward, and the π-bond propagates to the next C−C site (see structure d in Figures 9 and 10) which we can denote by $(C_1-C_2-C_3)^{\bullet}-(C_4-\mathbf{C_5}=\mathbf{C_6})^{\bullet}-(\mathbf{C_7}=C_8-C_9=C_{10}-C_{11}=C_{12})$. After ca. 40 fs this pattern then repeats itself to give

Chart 5

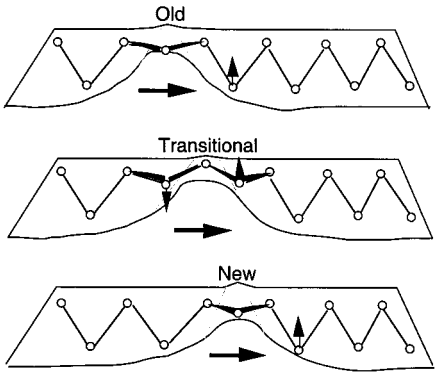

structure f, $(C_1{-}C_2{-}C_3)^{\bullet}{-}(C_4{-}C_5{=}C_6{-}\mathbf{C_7{=}C_8})^{\bullet}{-}(\mathbf{C_9{=}}C_{10}{-}C_{11}{=}C_{12})$ and again then structure h, $(C_1{-}C_2{-}C_3)^{\bullet}{-}(C_4{-}C_5{=}C_6{-}C_7{=}C_8{-}\mathbf{C_9{=}C_{10}})^{\bullet}{-}(\mathbf{C_{11}}{=}C_{12})$. After the end of the chain is reached, relaxation begins to occur in the final $(C_1{-}C_2{-}C_3)^{\bullet}{-}(C_4{-}C_5{=}C_6{-}C_7{=}C_8{-}C_9{=}C_{10}{-}C_{11}{=}C_{12})^{\bullet}$ closed-shell fragment. As shown in Figures 9 and 10, during this process a kink feature moves forward 7 −CH− units.

The mechanism of the motion in this trajectory involves the lowering of the old kink and the lifting of a new kink in an adjacent position, leading to a transitional structure where both kinks are lifted. This type of molecular motion resembles the wave that can be induced along *one* of the two edges of a long strip of fabric as illustrated in Chart 5.

The exchange density matrix provides a rationalization for this behavior. P_{ij} plots for the five central C−C bonds are shown in Figure 12. Again P_{ij} values of 1 and −0.5 correspond to perfect double bonds and single bonds, respectively. The reverse coupling is stable only for a very short time: after 39 fs the system switches toward the normal bond ordering as demonstrated by the crossing between the curves associated with the 4−5, 6−7 and 3−4, 5−6, 7−8 bonds. Due to this crossing, at ∼39 fs the spin coupling changes from that corresponding to a π-diradical to that corresponding to a closed-shell system. The force driving this process is obviously associated with the increase in the number of double bonds, which is three (three P_{ij} with values of ca. 1) rather than two after the crossing. Notice that in Figure 11 there are two lines with P_{ij} values of ca. 1 before the crossing and three after the crossing.

In the preceding discussion, we have described structure c as a transitional structure. Structure e, at 71 fs, represents another of these structures (whose position is indicated by dashed lines in Figure 11) where all C−C bonds (except the central and terminal C−C) have almost the same length. Structure e is associated with a large "pulse" (not a crossing) in all the major P_{ij} which become almost equal. After the pulse, the normal coupling is again dominant, and the chain has twisted again to bring the −(CHCH)− unit into the same plane as the previous double bond. As illustrated in Chart 5, this mechanism allows the kink to progress two carbon atoms along the chain, passing through a transitional structure as the P_{ij} pulse hits the molecule. This sequence of motions is repeated (see structures f−j) along the whole molecule in a wavelike motion until the kink reaches the end of the chain, and the standard bond alternation is fully restored (structure k). Thus, one can interpret the set of snapshots in four periodic cycles, as the kink travels along the chain: c−d → e−f → g−h → i−j. The first snapshot of each pair is a transitional structure, corresponding to one of the four P_{ij} pulses. The driving force pushing the kink ahead (from left to right in Figure 9 and from back to front in Figure 10) toward the end of the chain must be associated with the pressure for the construction of a longer conjugating chain segment at the left of the kink. The simultaneous rise of a new kink, one C−C unit ahead, may be a consequence of the wavelike motion associated with the conservation of momentum.

The trajectory just discussed features a kink propagation along the chain but with normal bond ordering. The mechanism shows how an initially generated inverted bond ordering is annihilated and driven back to the closed-shell coupling. Now let us consider a trajectory of type iii characterized by a longer lived π-diradical where the propagation also occurs along a chain with inverted coupling. In Figure 13 we show snapshots of the molecular

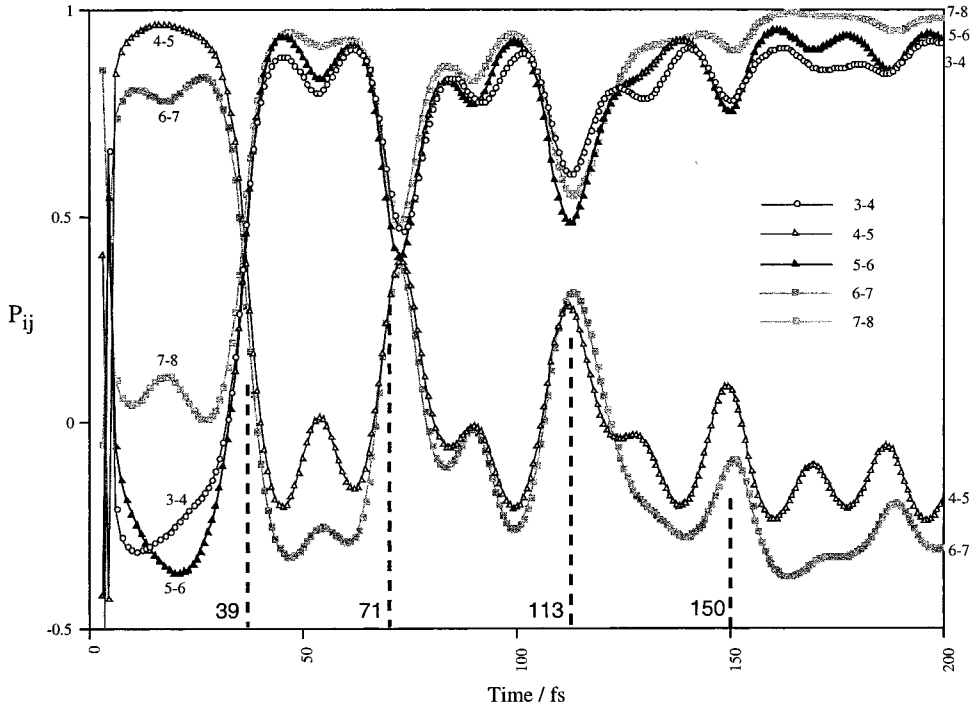

Figure 12. Exchange density data (P_{ij}) for the trajectory shown in Figures 9 and 10.

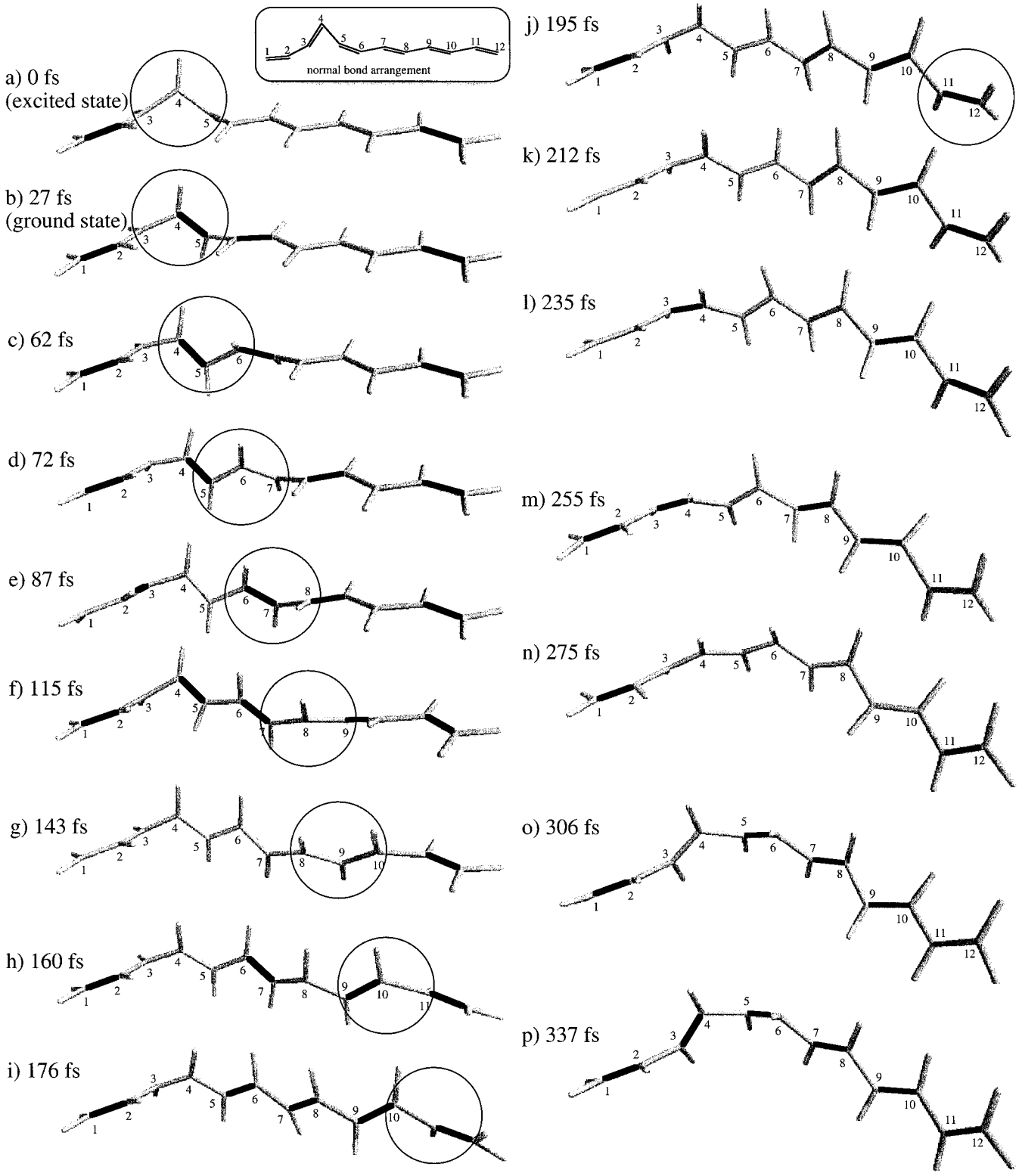

Figure 13. Snapshots from a $C_{12}H_{14}$ trajectory with a long inverted π-electron coupling lifetime. Bond lengths of less than 1.37 Å are indicated in bold. The kink is circled at each frame.

structure along the computed trajectory. The corresponding P_{ij} data are shown in Figure 14. The P_{ij} values reveal that, in this case, the inverted electron coupling is stable up to ~160 fs, after which the normal coupling pattern takes over and the plot behaves in a fashion similar to the trajectory of type ii. A strong P_{ij} pulse occurs at ~200 fs, producing a transitional structure as previously observed, and also at ~275 fs there is a similar structure, accompanied by a weaker P_{ij} pulse.

Examination of Figure 13 reveals that a kink also exists in the inverted bond order species. However, in this case the propagation appears to be more complex than that seen above for the closed-shell species. In particular, by inspection of structures b−h one can see that the transitional structure cannot be easily defined but seems to involve a larger portion of the chain. Thus, structure b, $(C_1{-}C_2{-}\mathbf{C_3})^{\bullet}{-}(\mathbf{C_4{=}C_5}){-}(C_6{=}C_7{-}C_8{-}C_9{-}C_{10}{-}C_{11}{=}C_{12})^{\bullet}$, propagates to d, $(C_1{-}C_2{-}C_3)^{\bullet}{-}(C_4{=}$

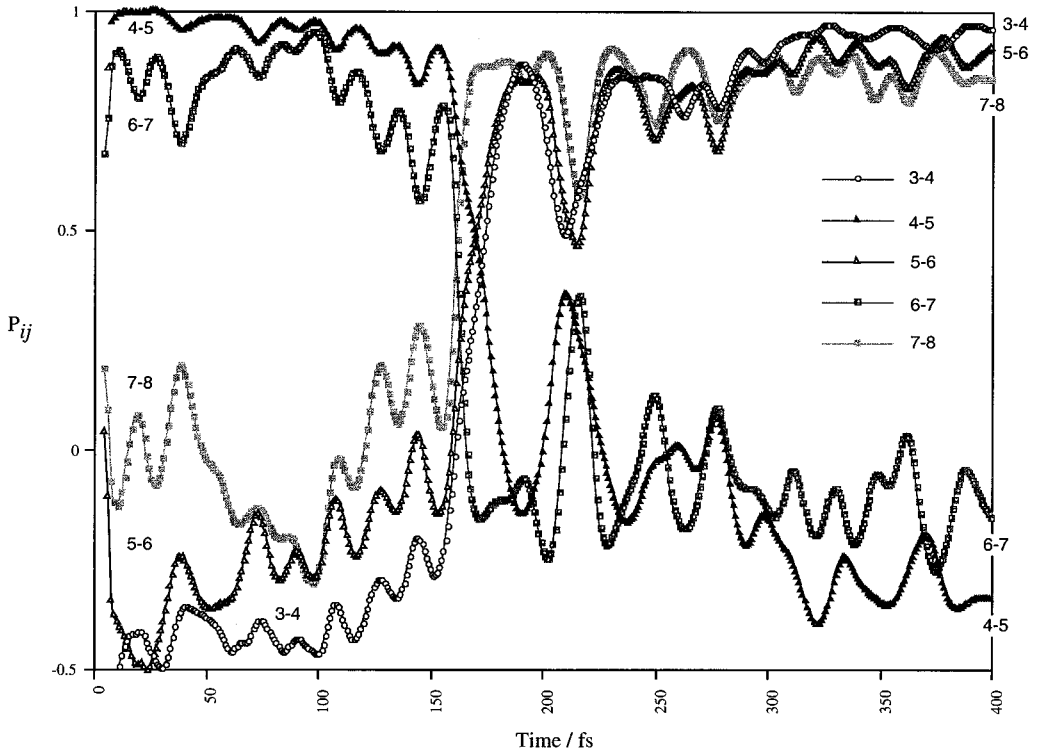

Figure 14. Exchange density data (P_{ij}) for the trajectory shown in Figure 13 with a long inverted π-electron coupling lifetime.

$\mathbf{C_5}-\mathbf{C_6})^{\bullet}-(\mathbf{C_7}-C_8=C_9-C_{10}-C_{11}=C_{12})$, and then to f, $(C_1-C_2-C_3)^{\bullet}-(C_4=C_5-C_6=\mathbf{C_7}-\mathbf{C_8})^{\bullet}-(\mathbf{C_9}=C_{10}-C_{11}=C_{12})$. In this case the driving force for the propagation seems to be associated with the expansion of the conjugated chain (with consequent stabilization of the radical center) at the left of the kink. Then, at ca. 160 fs, a cooperative vibration with associated P_{ij} value crossing is observed (see Figure 14) as in the previous example. Thus, this cooperative vibration (see also above) represents the general way in which the inverted bond ordering (i.e., the π-diradical) is annihilated.

If the type of propagation occurring before the 160 fs annihilation is continued (as happens in other trajectories), one ultimately gets $(C_1-C_2-C_3)^{\bullet}-(C_4=C_5-C_6=C_7-C_8=C_9-\mathbf{C_{10}}=\mathbf{C_{11}}-\mathbf{C_{12}})^{\bullet}$. In this structure, the $C_1\cdots C_3$ and $C_4\cdots C_{12}$ fragments are 90° twisted about the C_3-C_4 bond and the C_4-C_{12} radical segment can subsequently give structures similar to that shown in Figure 4c. This π-diradical structure then remains "dynamically locked" in skeletal vibrations for a long time (up to ca. 1 ps in our dynamic simulations), producing the type of trajectory reported in Figure 6. Indeed, the above trajectory shows that, in the first 160 fs, the skeletal vibrations are coupled to kink propagation, i.e., to a directionally ordered motion of the kink, which propagates reverse bond ordering along the chain. At 160 fs, in contrast, we see how (via a cooperative vibration) the inverted π-electron coupling is destroyed and the closed-shell coupled species is generated. Of course, in a very long chain, kink propagation coupled with skeletal vibration can continue indefinitely. *In particular, in a polymer, this quasi-periodic trajectory would propagate until a defect or the other kink is encountered.*

4. Conclusions

The word soliton implies nondispersive shape-conserving motion.[8] In the context of polymer physics, solitons correspond to vibrational distortion of a segment of the polymer chain usually formed through a perturbation of the polymer electronic structure. In the context of *trans*-polyacetylene, a long polyene chain, pairs of solitons occur as boundaries between the two possible bond alternation patterns.[9a]

The high-energy (HE) peak observed in *trans*-polyacetylene photoinduced absorption spectra has been associated with the generation of neutral soliton pairs, where a neutral soliton S^0 is a spin 1/2 species and a $\bar{S}^0$ is a spin $-1/2$ species.[7a−c,9a−d,16] Further, photogeneration of spin 1/2 species has been conclusively proved by light-induced electron spin resonance (LESR),[16d] which has been used to investigate the spin state of photoexcitations in conducting polymers. Finally, photoabsorption-detected magnetic resonance (ADMR)[9c,16a,b] has confirmed the existence of spin 1/2 neutral solitons−antisolitons with an optical transition at ∼1.4 eV: the HE band. Thus, neutral soliton−antisoliton pairs are the main result of *trans*-polyacetylene intrachain photoexcitation on short time scales.

In the context of organic chemistry, S^0 and $\bar{S}^0$ merely correspond to the radical centers of a π-diradical which necessarily comprise an inverted single bond/double bond pattern.[20] Thus, we believe that the transient π-diradical intermediate reported in section 3 for relatively short polyenes (up to six double bonds only) is a good model for the S^0 and $\bar{S}^0$ pair observed in *trans*-polyacetylene. In particular, in *trans*-polyacetylene as well as in simple polyenes, the $2A_g$ excited state (first investigated theoretically and then determined experimentally by Kohler et al.[7a−c]) is known to be located below the first optically allowed excited state $1B_u$. It has been suggested[7a,b,9d] that the HE peak may be due to an excitation from an electronic state analogous to the $2A_g$ state of short polyenes. This connection suggests a link between the $2A_g$ state (the S_1 state) and neutral soliton pairs. We believe that the nature of this link is clarified by the results presented above.

Many theoretical studies have been previously performed[9a−d,17−19] also simulating the role of doping agents and

(20) (a) Tolbert, L. M. *Acc. Chem. Res.* **1992**, *25*, 561. (b) Hoffman, R.; Janiak, C.; Kollmar, C. *Macromolecules* **1991**, *24*, 3725.

the transport of charge (via charged soliton−antisoliton pairs $S^+-\bar{S}^-$) along the polyacetylene chain axis. Most of them have used octatetraene and other longer polyenes as a first approximation model for polyacetylene.[17b] Most computations have assumed a planar model (ignoring three-dimensional interactions) and used simple model Hamiltonians (where electron−electron interactions and correlation effects have been ignored). In previous theoretical studies the term "defect" is usually used to imply a deformation (triggering soliton generation) within the plane of the molecule.

If we assume that our finite polyenes provide a reasonable model for the formation of neutral soliton pairs in polyacetylene, the results presented in section 3 strongly indicate that a planar model misses important paths.[9c,16c] In particular, we provide evidence that photochemical generation of $S^0-\bar{S}^0$ pairs proceeds via the $-(CH)_3-$ three-dimensional kink we observe in conical intersection geometries.[1] Thus, the concept of a planar geometrical kink propagating within the plane of the chain given in Chart 2 must be replaced by the picture of a localized out-of-plane kink moving, via ordered and concerted rotations of adjacent bonds, along the polyene chain. This effect may cause soliton motion and directionally ordered electron spin transport.

Acknowledgment. Computations were carried out, in part, on an IBM-SP2 funded jointly by IBM-UK and HEFCE (U.K.). This research has been supported by an EU TMR network grant (ERB 4061 PL95 1290, Quantum Chemistry for the Excited State) and Nato Grant CRG 950748.

Supporting Information Available: Text and figures describing the CAS−SCF reverse coupling MEP in *tEt*-hextriene and *tEtEt*-octatriene, MM−VB steepest descent lines for octatetraene and dodecahexaene, and MM−VB dynamics study of the relative stability of the reverse recoupling species (PDF). This material is available free of charge via the Internet at http://pubs.acs.org.

JA000385L